Int J Adv Manuf Technol (2017) 92:1991–2000
DOI 10.1007/s00170-017-0194-4

ORIGINAL ARTICLE

An approach on wheel position and orientation calculation for helical broaching tool sharpening

Kang Jia[1,2] · **Jun Hong**[1,2] · **Shuai Zheng**[1,2] · **Yinhang Zhang**[1]

Received: 24 July 2016 / Accepted: 20 February 2017 / Published online: 24 March 2017

Abstract Helical chip gullets play a crucial role in the performance of broaching tool. Well-sharpened helical rake flanks, which require accuracy of rake angle, smoothness of rake flank, and the safety of operators, are significantly to maintain its broaching performance. In this study, a wheel orientation and position calculating approach was developed to the resharpen of helical rake flank by a ring-like grind wheel. With modeling the process requirements of helical rake flank sharpening as the constraints like single side contacting and desired rotation direction of grinding wheel, the enveloping theory-based contact curve identification helped the wheel orientation calculation approximate to a nonlinear searching problem for easily addressing by Newton-Raphson method. Then, the analyses of contact curves with different wheel orientations and a ground helical rake flank proofed the sharpening process requirement was satisfied, and the examined results of rake angle for both ground rake flank and simulated bars verified the accuracy of the presented approach. At last, optimal grinding wheel setup that has taken larger wheel size and practicable orientation was suggested based on the relationship analysis among wheel radiuses and orientations.

Keywords Helical rake flank · Contact curve · Wheel orientation · Grinding process requirement · Orientation optimization

✉ Jun Hong
jhong@mail.xjtu.edu.cn

[1] School of Mechanical Engineering, Xi'an Jiaotong University, Xi'an 710049, People's Republic of China

[2] State Key Laboratory for Manufacturing System Engineering, Xi'an 710054, People's Republic of China

1 Introduction

Helical chip gullet is a significant structure of the broaching tools for chip curling and evacuation during broaching process. Comparing with the traditional ring-type gullets, the helical ones reduce the number of cutting teeth that engaging and withdrawing the workpiece, which effectively smooth the fluctuation of broaching force. The helical chip gullets also avoid the manufacture of chip break grooves. These benefits promote the work performance of broaching tool and enhance its economic. Commonly, the periodic sharpening of the helical rake flank is necessary to prolong the life of broaching tool and maintain the sharpness of cutting teeth. The parameters of broaching tool-like rake angle, core radius, and smoothness of the rake surface, which directly determine the cutting performance of the broaching tool, are generated in the rake flank sharpen, hence reasonable wheel position and orientation are significant to achieve the correct parameters.

As the foundation of helical gullet machining, figuring out the exact parameters of the helical gullet in transverse, i.e., rake angle and core radius and rolling angle are performed by analytical and discrete as well as CAD-based methods. The contact line of cutter was analytically identified with adopting envelop theory and differential geometry to described the transverse profiles of gullet [1–4]; however, it is complexity once singular points were existed. Nguyen and Ko [5] inserted effective cutting edge curves between singular points to complete the contact line, while Xiao et al. [6] detailed analyzed and calculated the contact line of grinding wheel as several curves. The profile of gullet can be identified by envelop these intersect curves via performing the helical gullet machining as the intersection between a given tool axial transverse and a serial of independent solid grinding wheels follow the cutting trajectory in Refs [7–10]. This discrete manner is effective to avoid the singular conditions occurred in

analytical methods, but the accuracy of profile was determined by the resolution ratio of numerical solution, and computed tasks are heavier. Furthermore, some CAD assisted methods taken using a Boolean operation to simulate the generation of helical gullet [11–13].

In order to achieve the desired transverse profile, either specifying the profiles of cutters or calculating the reasonable orientations and positions of cutters need to be taken. The cutter profile can be specified with respect that the rule that the contact points have the common surface normal between the cutter and desired gullet [14–17]. However, it will involve more machining operations and raise the cost. Comparatively, it is more attractive to adjusting the setup of cutter, which is generally performed as a searching problem that aims to minimize the difference between the designed flute parameters and the machined flute parameters. Karpuschewski et al. [18] proposed a particle swarm searching method to identify the reasonable setup of the grinding wheel, in which both the wheel orientation and position were adjusted to approximate the desired sectional profile. Rabahah and Chen [19] identified the orientation of the grinding wheel through matching its normal with the normal rake angle of the helical rake flank at first, and then fixed the wheel position by equaling the minimum distance between the effective grinding edge and the revolving axis to the core radius. Xiao et al. [6] also figured out the correct wheel setup condition with an iterative method, in which firstly estimated the sectional parameters by contact curve calculation, and Wang et al. [20] addressed this optimization in the basis of analyzing the geometric constraints like interferences avoidance and abnormal flute profile. With the helping of calculate the parameters of machined sectional profile by analytical methods, Ren et al. [21] directly formulated the correct wheel orientation as a nonlinear equation group and addressed by numerical solving. All these methods mainly focused on achieving the exactly parameters of machined sectional profile, but pay less attention on the guarantee the requirements of grinding process.

In practice, reasonable contact between the grinding wheel surface and rake flank is crucial to guarantee the smoothness of the ground rake flank and maintain the sharpness of the cutting edges. Therefore, in order to satisfy abovementioned sharpening process requirements as well as the safety of operators, a concise approach on calculation of the reasonable orientation and position of grinding wheel was developed in this study, and its optimal selection was also discussed accordingly. The remainder of this article was organized as follows. In Section 2, the basic mathematical models of the grinding wheel and its setup were established as well as the identification of the contact curves. In Section 3, the process requirements for rake flank sharpen was modeled, and the wheel orientation determination is performed. In Section 4, validations for proofing the distribution of contact line in terms of wheel orientation and examining the machined accuracy were reported, and the optimal selection of wheel orientation was also discussed. Finally, the conclusions were given.

2 Mathematical foundation of helical rake flank sharpening

2.1 Grinding wheel modeling

With considering the repetitive sharpening of rake flank and its economy, general cubic boron nitride (CBN) grinding wheels with annular shape are adopted to implement the rake flank grinding. Thereby, wheel profile dressing is avoided, and the management of wheel can be facilitated with assigned to specified broaching tools.

As the grinding wheel demonstrated in Fig. 1, a grinding wheel coordinate frame O_g-$X_gY_gZ_g$ is attached on it, where origin O_g coincides with the intersection point between the lateral surface of the wheel and its revolving axis, and Z_g-axis is coincided with the revolving axis of wheel, and X_g-axis and Y_g-axis are perpendicular to each other. Practically, only the arc-shape surface participates to the grinding task, so it is easy to express the grinding surface and its surface normal vector as in Eqs. (1) and (2), respectively.

$$S_g(\theta,\varphi)=\begin{bmatrix}\left(r_g\cos(\theta)+R_g\right)\cdot\cos(\varphi)\\ \left(r_g\cos(\theta)+R_g\right)\cdot\sin(\varphi)\\ r_g\cdot\sin(\theta)\\ 1\end{bmatrix} \tag{1}$$

$$N_s(\theta,\varphi)=\begin{bmatrix}\cos(\theta)\cdot\cos(\varphi)\\ \cos(\theta)\cdot\sin(\varphi)\\ \sin(\theta)\\ 0\end{bmatrix} \tag{2}$$

Where R_g is the major radius of the grinding wheel, r_g is the radius of the fillet, $\theta\in[-\pi/2,\pi/2]$, and $\varphi\in[0,2\pi)$.

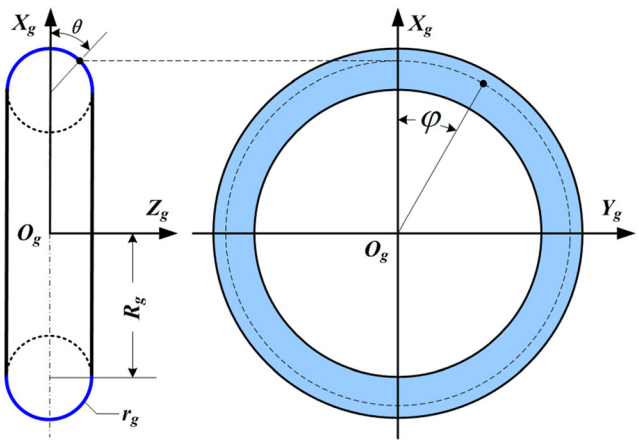

Fig. 1 Shape of the CBN grinding wheel

2.2 Wheel setup for helical rake flank sharpening

As shown in Fig. 2a, the broaching tool coordinate frame O_b-$X_bY_bZ_b$ is defined firstly to describe the helical rake flank sharpening process, where origin O_b attaches to the revolving axis of broaching tool, and Z_b-axis coincides with the revolving axis of broaching tool, X_b-axis and Y_b-axis are perpendicular to each other.

In practical, supporting fixes are located around the lower part of the broaching tool; hence, it is proper to place the grinding wheel on the upper side of the broaching tool, and it also facilitates the observation and adjustment for the operators. Therefore, the wheel position is defined by (Ax, Ay), which are the X-component and Y-component of O_g in broaching tool coordinate frame, respectively. Simultaneously, the wheel's orientation is fixed by rotating Σ along X_g-axis at first, and follows the rotation λ along Y_g-axis. Then, the wheel's setup is confirmed by Ax, Ay, Σ, and λ. Hereto, the transform matrix ${M_b}^g$ that from a grinding wheel coordinate frame to the broaching tool coordinate frame can be expressed as follows:

$$
\begin{aligned}
{M_b}^g &= \mathrm{tran}(\mathrm{Ax},\mathrm{Ay},0)\cdot\mathrm{rot}(X,\Sigma)\cdot\mathrm{rot}(Y,\lambda) \\
&= \begin{bmatrix} \cos(\lambda) & 0 & \sin\lambda & \mathrm{Ax} \\ \sin(\Sigma)\cdot\sin(\lambda) & \cos(\Sigma) & -\sin(\Sigma)\cdot\cos(\lambda) & \mathrm{Ay} \\ -\cos(\Sigma)\cdot\sin(\lambda) & \sin(\Sigma) & \cos(\Sigma)\cdot\cos(\lambda) & 0 \\ 0 & 0 & 0 & 1 \end{bmatrix}
\end{aligned} \tag{3}
$$

During helical rake flank grinding process, the grinding wheel implements a spiral motion relative to the broaching tool with accompanying a high-speed self-rotation. The relative spiral motion consists of a rotational motion along Z_b-axis and a synchronic linear motion along Z_b-axis. Hence, the relative spiral motion, which is a function of time t, can be expressed as in Eq. (4):

$$
M(t) = \begin{bmatrix} \cos(t) & -\sin(t) & 0 & 0 \\ \sin(t) & \cos(t) & 0 & 0 \\ 0 & 0 & 1 & \pm L_b\cdot t \big/ (2\pi) \\ 0 & 0 & 0 & 1 \end{bmatrix} \tag{4}
$$

Where L_b is the lead of the helical chip gullet, and the upper sign is used for the right-hand rotated gullet while the lower sign is used for the left-hand rotated gullet.

Thus, the grinding surface of wheel at t in broaching tool coordinate frame ${S_g}^b(\theta,\varphi,t)$ can be identified as follows:

$$
{S_g}^{\mathrm{b}}(\theta,\varphi,t) = M(t){M_b}^g S_g(\theta,\varphi) = \begin{bmatrix} x_s(\theta,\varphi,t) \\ y_s(\theta,\varphi,t) \\ z_s(\theta,\varphi,t) \\ 1 \end{bmatrix} \tag{5}
$$

Similarly, the normal vector of the grinding wheel surface ${N_g}^b(\theta,\varphi,t)$ at moment t in broaching tool coordinate frame can be identified as follows:

$$
{N_g}^{\mathrm{b}}(\theta,\varphi,t) = M(t){M_b}^g N_g(\theta,\varphi) = \begin{bmatrix} x_n(\theta,\varphi,t) \\ y_n(\theta,\varphi,t) \\ z_n(\theta,\varphi,t) \\ 0 \end{bmatrix} \tag{6}
$$

2.3 Grinding contact line determining

Taking specified orientation as illustrated in Fig. 3a, the swept volume of grinding wheel that produced by the relative spiral motion generates the helical rake flank. It indicates part of the external surface of the swept volume is same as the ground rake flank. At any moment of machining, the grinding wheel contacts the helical rake flank at a curve as drawn in Fig. 3d,

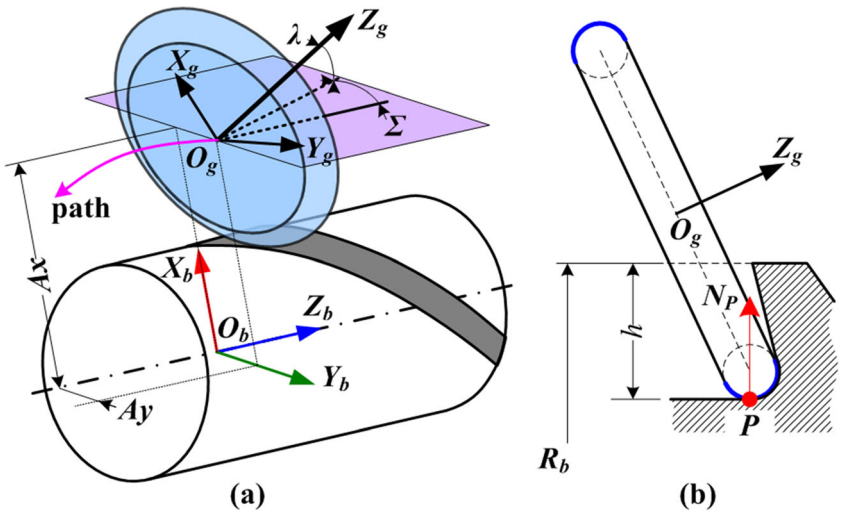

Fig. 2 Setup of the grinding wheel **a** the coordinate frames of the wheel and broaching tool and **b** the contact condition of the wheel

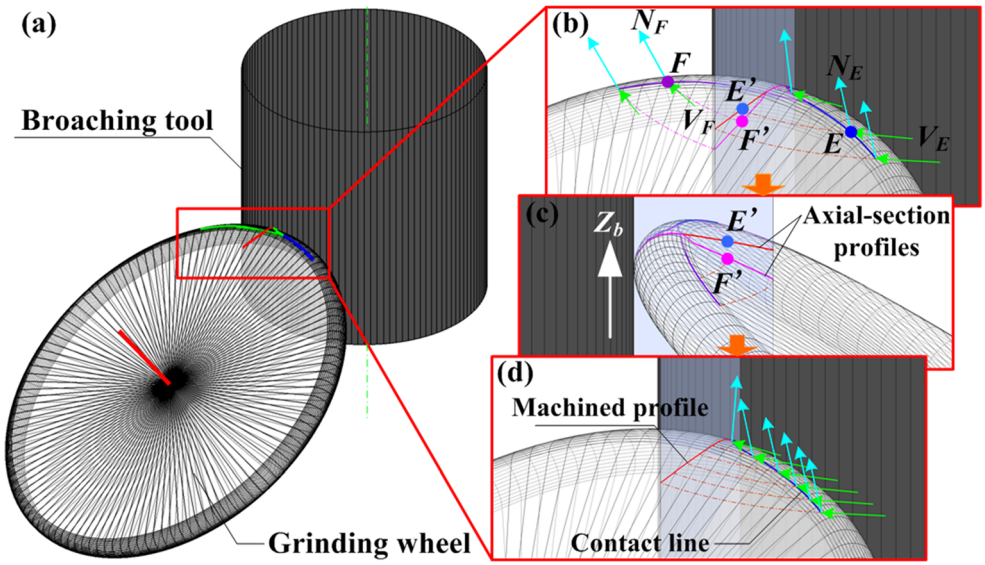

Fig. 3 Identification of the contact line

which is called the contact curve at current moment. In the basis of enveloping theory, we can identify this contact curve with the rule that the normal vectors of wheel at any contact points perpendicular to the corresponding wheel's velocities with respect the relative spiral motion. Accordingly, the points on the wheel surface that satisfies Eq. (7) compose the contact curve, and it can be solved by numerical methods.

$$V_g{}^b(\theta,\varphi,t)\cdot N_g{}^b(\theta,\varphi,t)=0 \tag{7}$$

Where, $V_g{}^b$ is the velocity of a point on the wheel surface in the broaching tool coordinate frame, and it is determined as:

$$V_g{}^b(\theta,\varphi,t)=\frac{\partial M(t)}{\partial t}M_b{}^g S_g(\theta,\varphi) \tag{8}$$

However, it needs attention that two potential solutions, i.e., points $E = [x_E(\theta,\varphi,t),\ y_E(\theta,\varphi,t),\ z_E(\theta,\varphi,t),1]^T$, and $F = [x_F(\theta,\varphi,t),\ y_F(\theta,\varphi,t),\ z_F(\theta,\varphi,t),1]^T$ take the same radius in wheel surface (see in Fig. 3b), and they are placed on both side of the wheel independently. Relative to the flat surface of the grinding wheel, the spiral motion generates two locally convex areas and fake contact point is brought.

Apparently, the truthful contact point can be identified through the judgment of axial relative position in axial-section plane as in Fig. 3c. Firstly, transforming both points E and F into an axial-section plane along the spiral motion, corresponding points $E' = [x_{E'},y_{E'},z_{E'},1]^T$ and $F' = [x_{F'},y_{F'},z_{F'},1]^T$ can be calculated by Eq. (9).

$$\begin{cases} E' = M(t_1)\cdot E \\ F' = M(t_2)\cdot F \end{cases} \tag{9}$$

Where, $t_1 = \pm\arctan(y_E/x_E)$ and $t_2 = \pm\arctan(y_F/x_F)$. The upper sign is used for the right-hand rotated helical gullet, and the lower sign is used for the left-rotated helical gullet.

Since the one with larger axial value takes effect in machining, the point whose axial-section point satisfies $\max(z_E, z_F)$ is confirmed as contact point. Furthermore, the contact curve is composed by a serial of contact points as illustrated in Fig. 3d.

2.4 Determination of rake angle

Rake angle as an important parameter of cutting teeth is defined depend on the ground rake flank. As shown in Fig. 4, P and Q are the points on the rake flank at radius R_b and R_r in the same axial-section plane. The section angle between QP and X_b-axis is defined as the rake angle γ of cutting teeth.

Therefore, at moment $t = 0$, points $M = [x_M(\theta,\varphi,t),\ y_M(\theta,\varphi,t),\ z_M(\theta,\varphi,t),1]^T$, and $N = [x_N(\theta,\varphi,t),\ y_N(\theta,\varphi,t),\ z_N(\theta,\varphi,t),1]^T$ on the contact curve MN, whose radius corresponding to R_b and R_r, can be identified by solving equation groups (9) and (10), respectively.

$$f_1(\theta,\varphi,t)\big|_{t=0} = \begin{cases} V_M(\theta,\varphi,t)\ \cdot\ N_M(\theta,\varphi,t) = 0 \\ \sqrt{x_m(\theta,\varphi,t)^2 + y_m(\theta,\varphi,t)^2} = R_t \end{cases} \tag{10}$$

$$f_2(\theta,\varphi,t)\big|_{t=0} = \begin{cases} V_N(\theta,\varphi,t)\ \cdot\ N_N(\theta,\varphi,t) = 0 \\ \sqrt{x_N(\theta,\varphi,t)^2 + y_N(\theta,\varphi,t)^2} = R_r \end{cases} \tag{11}$$

Obviously, these two transcendental equation groups can be fixed by adopting Newton-Raphson method in form of numerical solution. Next, for points M and N, their

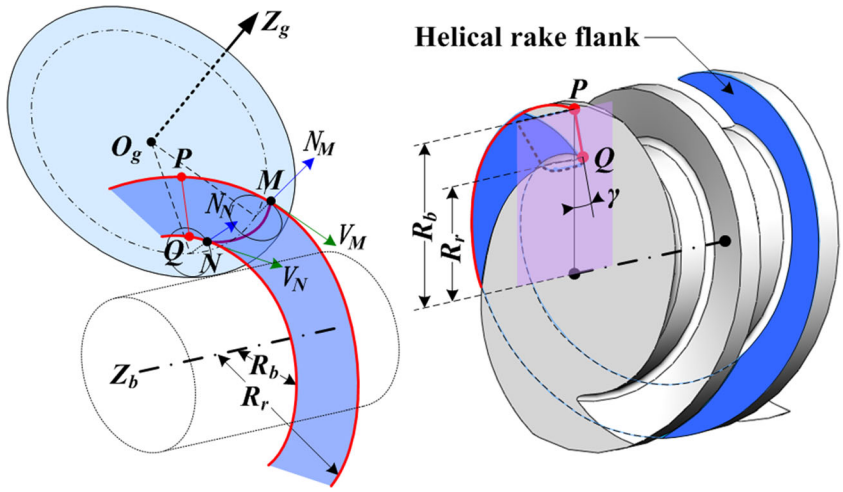

Fig. 4 Definition and calculation of the rake angle

corresponding points P and Q following the spiral motion are identified as Eq. (9). Then, the rake angle γ is determined by Eq. (12), and its sign is same as the third component of QP.

$$\gamma = \arccos\left(\frac{\mathrm{QP}\cdot[1,0,0,0]^{\mathrm{T}}}{|\mathrm{QP}|}\right) \tag{12}$$

3 Wheel's position and orientation identification

For the sake of helical rake flank resharpen, reasonable position and orientation of the grinding wheel directly determines the correct generation of helical rake flank related parameters like rake angle, core radius, and so on. However, the process requirements of rake flank grinding also play a crucial role in maintain the ground surface quality, and they deserve serious consideration.

3.1 Grinding process constraints modeling

3.1.1 Radius of gullet bottom guaranteeing

In sharpening, grinding wheel touches both the rake flank and bottom surface of chip gullet as depicted in Fig. 2b, which leads to uniform material removal and generates a smooth arc at the corner of chip gullet. It indicates the wheel should tangent the bottom surface of the chip gullet at point P. For simplicity, we suppose $P = [R_b\text{–}h,0,0,1]^{\mathrm{T}}$ going through X_b-axis at initial time $t = 0$, thereby the initial position (Ax and Ay) of the grinding wheel can be figured out.

It is clearly to identify the normal vector $N_P = [1,0,0,0]^{\mathrm{T}}$ of point P, and the normal vector of the contact point on grind wheel surface coincides with it as in Eq. (13).

$$N_g{}^b(\theta,\varphi,t)\Big|_{t=0} = [-1,0,0,0]^T \tag{13}$$

With respect of the geometry of grind wheel, we can deduce that the contact point must be located in the lower part of the grinding wheel, and it can be determined as, $\theta = -\lambda$and $\varphi = \pi$through satisfying Eq. (8).

$$S_g{}^b(\theta,\varphi,t)\Big|_{\theta=\lambda,\varphi=\pi,t=0} = [R_b\text{–}h,0,0,1]^T \tag{14}$$

Accordingly, the initial setting position of the grinding wheel (Ax, Ay) can be easily figured out as follows:

$$\begin{cases} \mathrm{Ax} = R_b - h + \cos(\lambda)\cdot R_g + r_g \\ \mathrm{Ay} = \sin(\Sigma)\cdot\sin(\lambda)\cdot R_g \end{cases} \tag{15}$$

3.1.2 Contact area for the grinding wheel and the rake flank

In order to promote the smoothness of ground rake flank and ensure the sharpness of cutting edges, the grinding wheel is asked to contact the rake flank only at the side that the cutting speeds point from the tip of cutting teeth to the bottom of the chip gullet. Furthermore, the grinding speed of wheel should depart away the operators with respect their safety. Thus, reasonable orientation of grinding wheel as well as its rotated direction should satisfy these requirements.

In practical applications, the combination of chip gullet rotate direction (right and left hand) and rotated direction of grinding wheel (clockwise and anti-clockwise) consists of four types of cases as described in Fig. 4a. Obviously, reasonable orientation angle Σ is necessary to meet the desired one side contact and expected cutting speed direction. Besides, in the basis of the structure of helical chip gullet, the helix angle of rake flank is varying with the radius. As exhibited in Fig. 4b, the minimum helix angle β_b appears at the bottom of the chip gullet, while the maximum one β_t produces at the tip of cutting teeth.

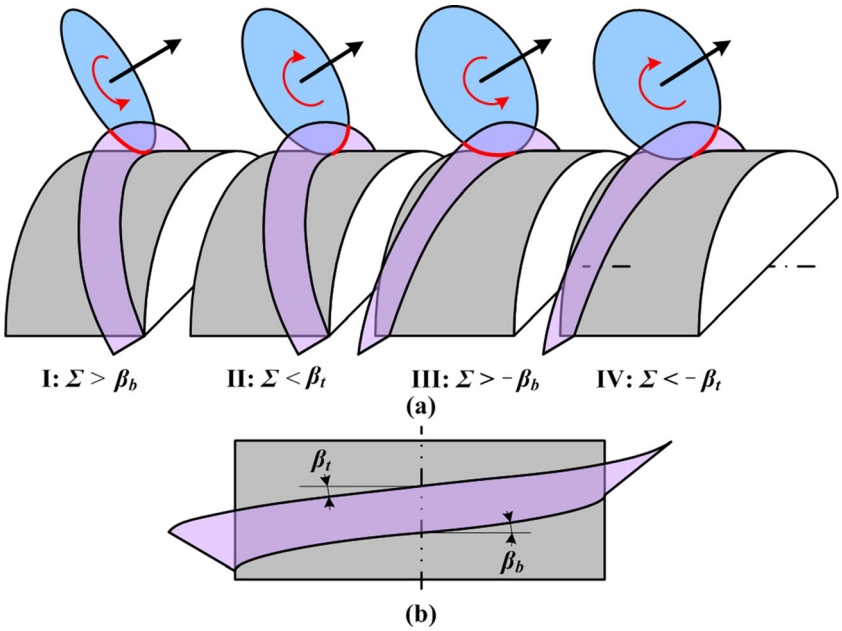

Fig. 5 Work condition and initial setup condition of the grinding wheel **a** the working condition of the grinding wheel and **b** the helix angles in radial direction

Intuitively, the orientation angle Σ should escape the range $[\beta_t, \beta_b]$ ($[-\beta_b,-\beta_t]$ for the left-hand rotate gullet) to satisfy the one-side contact condition. Without losing the practicability, Σ is initialized as follows. At first, we identify the rotate direction of grinding wheel according to the rotation of the gullet and the operator position. Then assigning the initial Σ as depicted in Fig. 5a, i.e., $\Sigma = \beta_b$ for case I, $\Sigma = \beta_t$ for case II, $\Sigma = -\beta_t$ for case III, and $\Sigma = -\beta_b$ for case IV. Afterward, Σ is adjusted to depart from the range $[\beta_t, \beta_b]$ (or $[-\beta_b,-\beta_t]$) until the one-side contact condition is satisfied with the help of contact condition indication in following subsection.

3.1.3 Wheel contact condition indicating

As forementioned in Section 2.3, contact line consist of a serial of points, and the coordinate of each point $C = [x_C(\theta,\varphi,t), y_C(\theta,\varphi,t), z_C(\theta,\varphi,t), 1]^T$ is confirmed. Then, the single-side contact condition equals to an inequality as follows:

$$\pm y_C(\theta, \varphi, t) > 0 \tag{16}$$

Where, the upper sign corresponding to cases I and III, and the lower sign corresponding to cases II and IV in Fig. 5a.

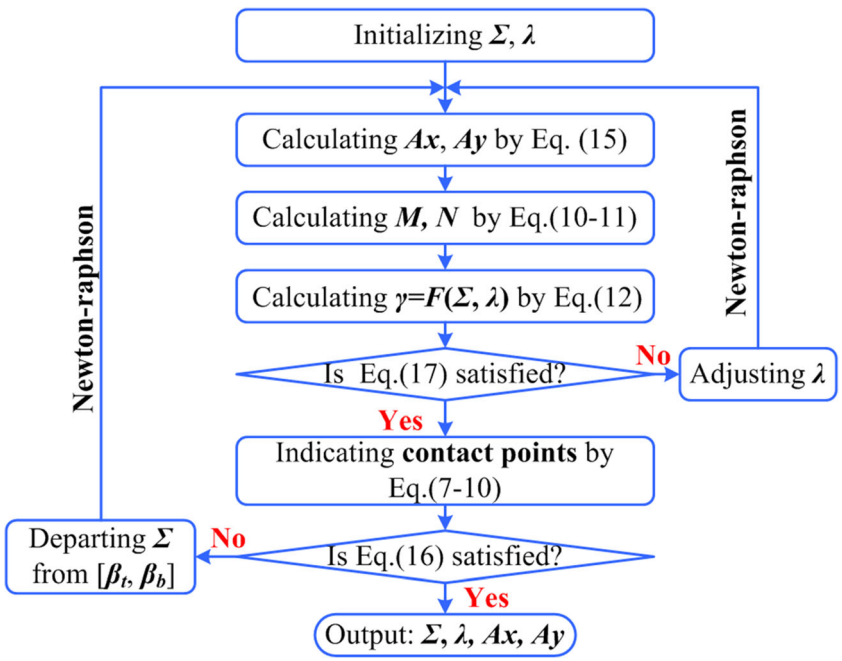

Fig. 6 Flowchart of the grinding wheel orientation calculation

Table. 1 The parameters of machined helical broaching tool

L_b (mm)	Rotated direction	R_b (mm)	R_r (mm)	h (mm)	γ_d (°)
50.8	Right hand	73	70	8.0	18

3.2 Determination of wheel's orientation

The machined rake angle is modeled as a function in terms of a wheel orientation in Section 2.4, consequently, wheel setup for the desired rake angle equals to nonlinear Eq. (17) with subject inequality (16).

$$G(\Sigma, \lambda, \gamma_d) = \gamma(\Sigma, \lambda) - \gamma_d = 0 \tag{17}$$

It can be fixed as an optimal question according to the flowchart in Fig. 6. Initializing the orientation angle (Σ, λ) as discussion in Section 3.1.2, and then the wheel position and brought rake angle can be identified. Iterative searching (like Newton-Raphson method) is performed till Eq. (17) is satisfied with adjusting λ. Then, with adopting inequality (16), the single-side contact of contact curve is discriminated, and the suitable wheel orientation is determined when this condition is met else Σ is revised as stay away the range $[\beta_t, \beta_b]$. Essentially, this problem translates the searching of λ and Σ in two different leveling, and reduces the complexity of calculation.

Table. 2 The setup of grinding wheel for validations

No.	γ (°)	Σ (°)	λ (°)	Ax (mm)	Ay (mm)
1	18	6.100	33.992	118.434	4.456
	18	6.700	38.953	114.574	5.501
	18	7.320	41.308	112.588	6.308
2	12	7.320	29.395	121.594	4.690
	15	7.320	35.340	117.430	5.5274
	18	7.320	41.308	112.588	6.3079

4 Examples and discussions

4.1 Verifications

The sharpening task for a helical broaching tool was implemented to verify the feasibility of the proposed method. The parameters of this broaching tool were listed in Table. 1, and key parameters of used CBN grinding wheel were R_g = 50 mm, and r_g = 1.25 mm.

Firstly, in order to demonstrate the effect of wheel orientation on the contact curve, the virtual helical rake flank ground with different Σ was illustrated in Fig. 7, and adopted wheel setups were group 1 in Table. 2. The contact line MN was totally placed on the cutting speed exiting side as in Fig. 7a where $\Sigma < \beta_t$, while the contact line MN was distributed on both sides of the grinding wheel as in Fig. 7b where $\beta_t < \Sigma < \beta_b$, and the contact line MN perfectly located on the cutting speed engaging side as in Fig. 7c where $\beta_b < \Sigma$.

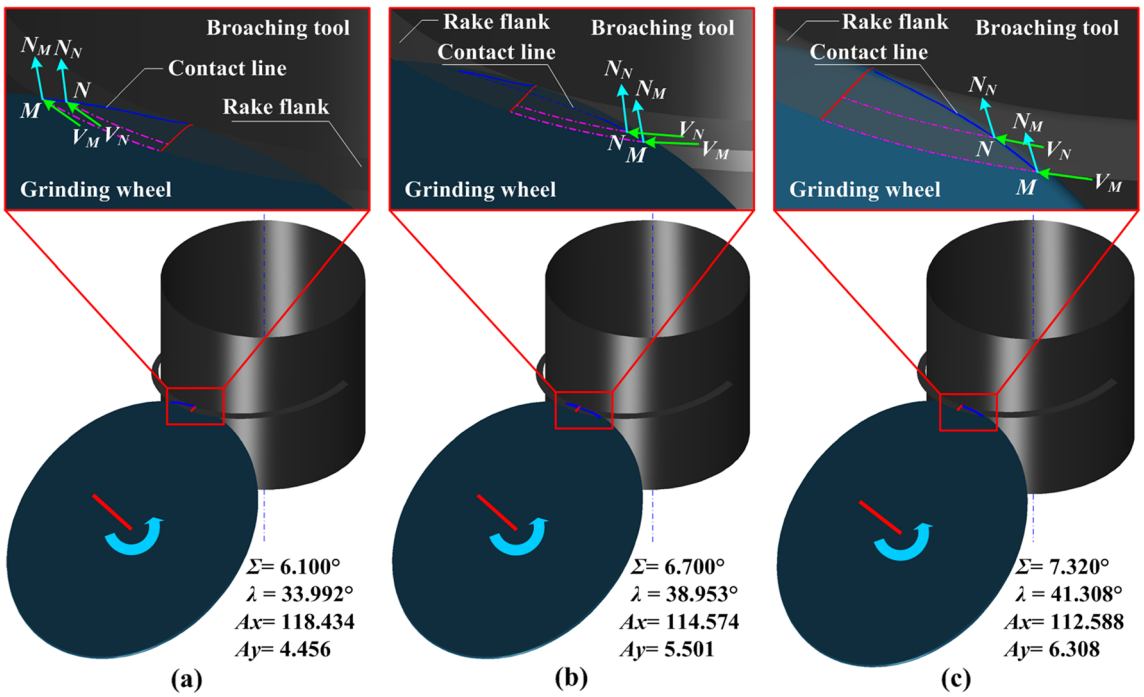

Fig. 7 Virtual grinding of rake flank **a** wheel takes Σ = 6.100° and **b** wheel takes Σ = 6.700° and **c** wheel takes Σ = 7.320°

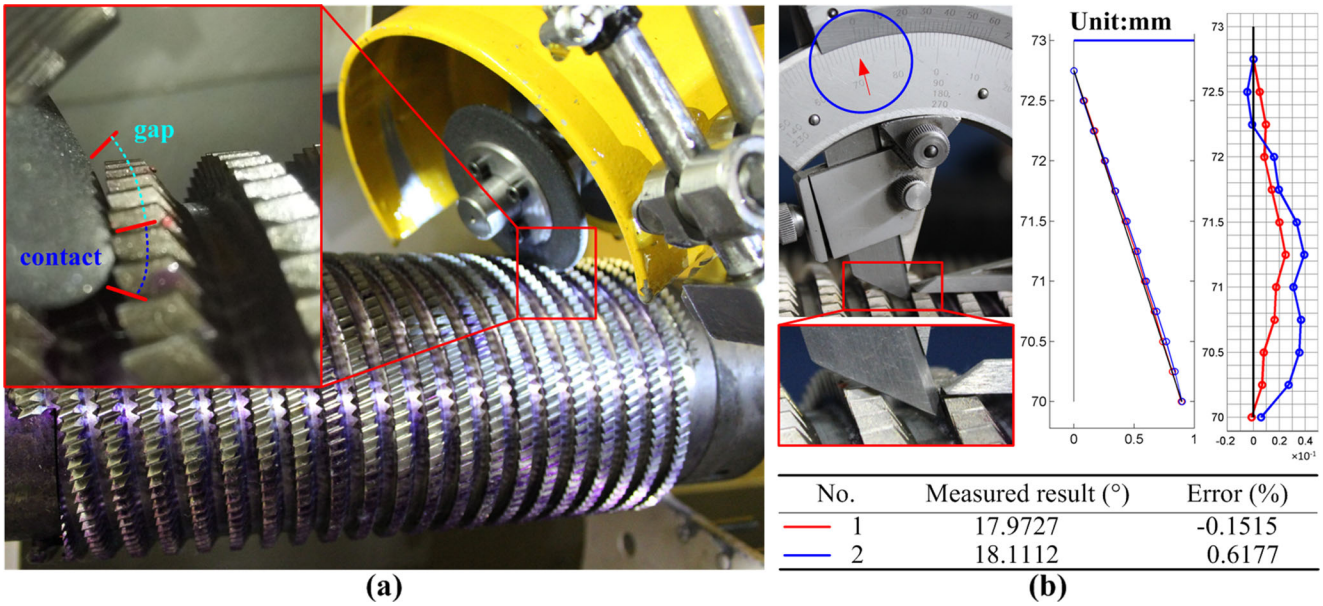

No.	Measured result (°)	Error (%)
1	17.9727	-0.1515
2	18.1112	0.6177

Fig. 8 Verification of a ground helical rake flank **a** the working status and **b** the inspected rake angles of ground rake flank

Moreover, in order to proof the accuracy of the method, both ground helical rake flank and serial of CAD simulated results are investigated. At first, the grinding status of the rake flank was depicted in Fig. 8a, there the arc part of grinding wheel contacted the helical rake surface in the engage side while leaved a gap on the exit side. Both the goniometer and probe sampled axial-section profiles reported the consistent 18° rake angles, and errors less than 1% were shown in Fig. 8b. Meanwhile, the machining of helical rake flanks on a bar with the same parameters as in Table 1 but taken different rake angles γ were simulated by VERICUT. With performing the wheel's setups as group 2 in Table .2, the machined helical gullets were drawn in Fig. 9, and the errors of examined rake angles (in Pro/E) were also no more than 1%.

Overall, the correct distribution of wheel contact as well as the exactly rake angles demonstrated in those validations verified the proposed method was capable to provide reasonable orientation of grinding wheel for helical rake flank sharpening of the broaching tool.

4.2 Optimal selection of the wheel orientation

Evidently, lots of wheel orientations satisfy the sharpening of rake flank. However, several factors deserve notice for wheel orientation choosing in practice. At first, wheel orientation angles shall inner the feasible ranges of machine tool. Secondly, larger radius wheel is preferred because of it brings longer service life, and it also reduces the highest rotation speed requirement of spindle. Thirdly, smaller λ is expected

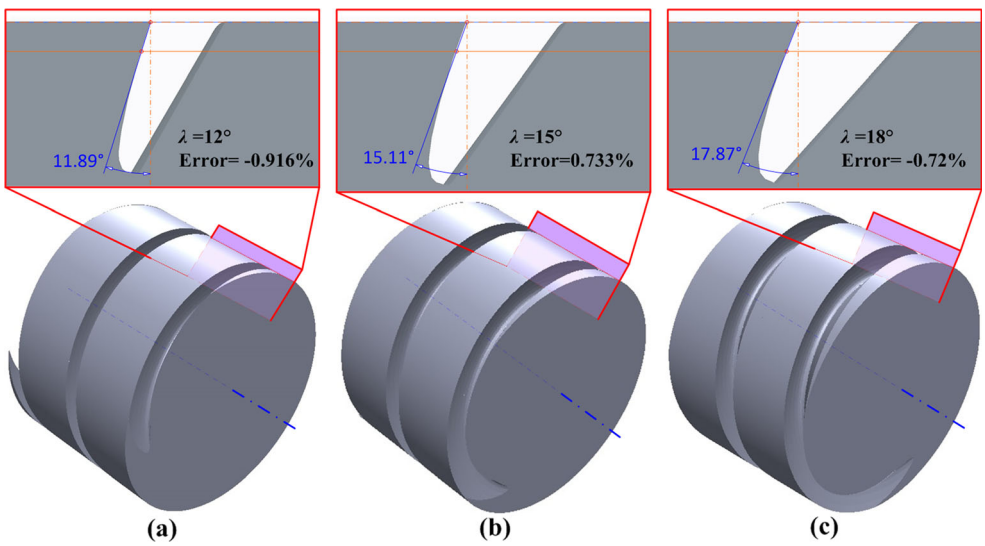

Fig. 9 CAD based validation and examining

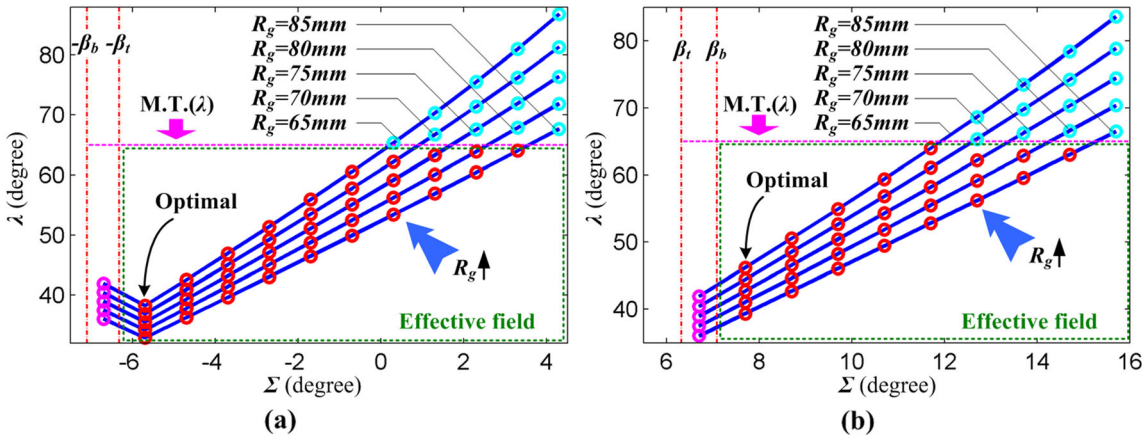

Fig. 10 Relationship between the orientation and size of the grinding wheel **a** the left-hand rotated helical rake flank and **b** the right-hand rotated helical rake flank

since it benefits of interference avoiding between the grinding wheel and the rear surface of front cutting tooth. Thus, analyzing the distribution of effective wheel orientations is significant for wheel's orientation optimal.

Performing the same sharpen task as in Table. 1 (adopt both left/right hand rotation), we identified all the wheel orientations (angle λ) in terms of discrete Σ and R_g, and demonstrated both the results for left-hand rotated gullet in Fig. 10a and the right-hand rotated gullet's in Fig.10b, respectively. It obviously that, for both situations, the increasing of λ was consistent with the greatening of Σ. Moreover, the amplified R_g enhanced the raising of Σ in further. Concurrently, we can identify the feasible wheel orientations by two conditions. One of them was the limitation of machine tool (e.g., $\lambda < 65°$), which get rid of those ones require oversized λ, and the other one was the critical Σ to ensure the single-side contact condition, i.e., $(\Sigma > -\beta_t)$ for the left-hand rotate gullet and $(\Sigma > \beta_b)$ for the right-hand rotate gullet in current task.

Consequently, we can deduce that the one taken the largest radius and feasible Σ close to the helix angle was optimal,

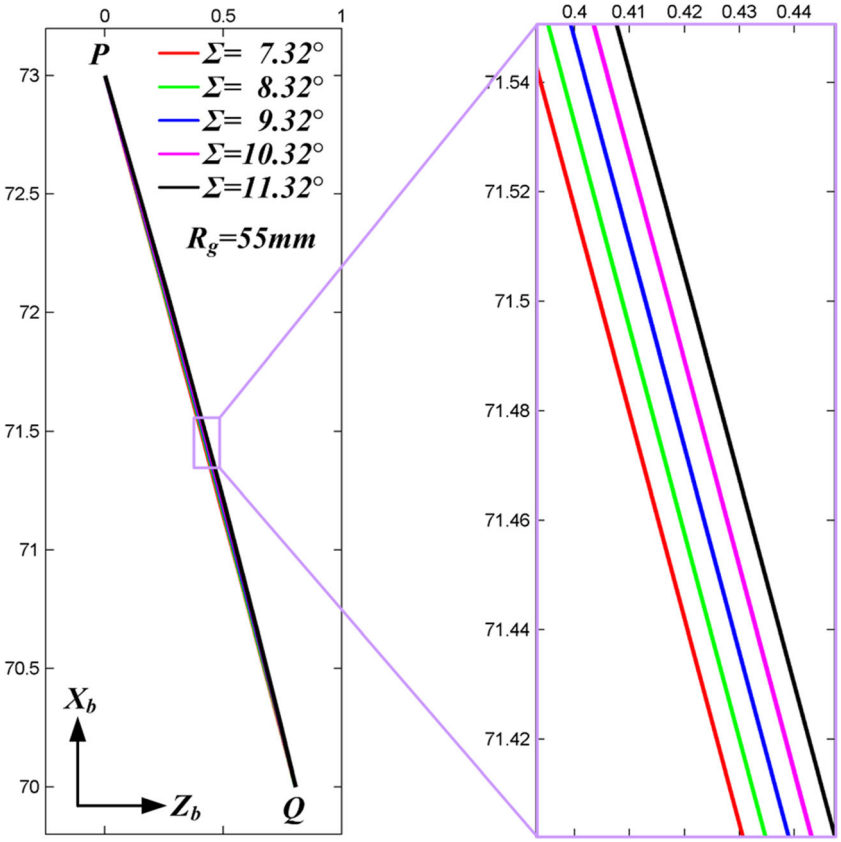

Fig. 11 Axial-section profiles of the rake flank with different wheel orientations

through considering the abovementioned factors like larger wheel radius, smaller λ as well as the feasibility of wheel orientation (Σ, λ). Similarly, the orientation that Σ close to the helix angle was optimal even without considering the variation of wheel radius.

Furthermore, we also analyzed the geometrical variations of the rake flank in axial section. These deviations were brought by contact curves that generated by unique wheel orientation. The detailed axial section profiles in Fig. 11 exhibited larger Σ produced more concave of MN. However, these tiny deviations, which totally no more than 20 um, were so small that have no evident effect on the working performance of rake flank. Then this geometrical deviation about Σ can be ignored.

5 Conclusions

This study proposed a wheel's orientation and position calculate method for helical rake flank sharpening of the broaching tool with respected that the corresponding requirements of grinding process, and the optimal orientation selection was also recommended. In detail, the contact points were geometrical discriminated by the axial positions in the axial-section among the local extremum that obtained by the envelop theory, then the process requirements of rake flank sharpening were modeled as a single-contact condition as well as the rotate direction of grinding wheel. Consequently, the initial Σ was assigned to the helix angle of rake flank like $\pm\beta_t$ ($\pm\beta_b$) for wheel orientation calculation, which was modeled as a nonlinear equation group and solved by Newton-Raphson method. The geometrical validations for contact curve distributing of wheel with different orientations proofed reasonable Σ could guarantee the single-contact condition, and it was consistent with the truthful machining status. Moreover, the examination of machined rake angle for both ground helical rake flank and simulated bars reported the error overall being less than 1%. At last, in practice, Σ that approximated to the helix angle of rake flank (like β_t or β_b) will meet the process requirements that were suggested as the optimal wheel orientation to achieve a smaller λ for interference avoidance. Furthermore, larger wheel radius was also preferred to enlarge its service life.

Acknowledgement The author is grateful to the editor Andrew Y C Nee and the anonymous referees for their helpful suggestions, which greatly help in improving the quality of this paper, and also would like to thanks the financial support by the National Natural Science Foundation of China (Grant No. 51421004), and National Key Technologies R&D Program of China (Grant No. 2015ZX04014021).

References

1. Ehmann KF, De Vries MF (1990) Grinding wheel profile definition for the manufacture of drill flutes. CIRP Ann—Manuf Technol 39(1):153–156
2. Sheth DS, Malkin S (1990) CAD/CAM for geometry and process analysis of helical groove machining. CIRP Ann—Manuf Technol 39(1):129–132
3. Kang SK, Ehmann KF, Lin C (1996) A CAD approach to helical groove machining. Part 1: mathematical model and model solution. Int J Mach Tools Manuf 36(1):141–153
4. Zhang W, Wang X, He F, Xiong D (2006) A practical method of modelling and simulation for drill fluting. Int J Mach Tools Manuf 46(6):667–672. doi:10.1016/j.ijmachtools.2005.07.007
5. Nguyen VH, Ko SL (2013) Determination of workpiece profile and influence of singular point in helical grooving. CIRP Ann—Manuf Technol 62:323–326. doi:10.1016/j.cirp.2013.03.009
6. Xiao S, Wang L, Chen ZC, Wang S, Tan A (2013) A new and accurate mathematical model for computer numerically controlled programming of 4Y1 wheels in 2½-axis flute grinding of cylindrical end-mills. J Manuf Sci Eng 135:41008
7. Kaldor S, Rafael AM, Messinger D (1988) On the CAD of profiles for cutters and helical flutes—geometrical aspects. CIRP Ann—Manuf Technol 37(1):53–56
8. Ko SL (1994) Geometrical analysis of helical flute grinding and application to end mill. Transactions of NAMRI/SME 12:165–172
9. Puig A, Perez-Vidal L, Tost D (2003) 3D simulation of tool machining. Comput Graph 27(1):99–106
10. Li G, Sun J, Li J (2014) Modeling and analysis of helical groove grinding in end mill machining. J Mater Process Technol 214:3067–3076. doi:10.1016/j.jmatprotec.2014.07.009
11. Ivanov V, Nankov G, Kirov V (1998) CAD orientated mathematical model for determination of profile helical surfaces. Int J Mach Tools Manuf 38:1001–1015. doi:10.1016/S0890-6955(98)00002-9
12. Mohan LV, Shunmugam MS (2004) CAD approach for simulation of generation machining and identification of contact lines. Int J Mach Tools Manuf 44:717–723. doi:10.1016/j.ijmachtools.2004.02.013
13. Kim JH, Park JW, Ko TJ (2008) End mill design and machining via cutting simulation. Comput Des 40:324–333. doi:10.1016/j.cad.2007.11.005
14. Xiao DC, Lee C (1994) A contact point method for the design of form cutters for helical gears. J Eng Ind 116:387–391
15. Feng X, Hongzan B (2003) CNC rake grinding for a taper ball-end mill with a torus-shaped grinding wheel. Int J Adv Manuf Technol 21(8):549–555
16. Hsieh J, Tsai Y (2006) Geometric modeling and grinder design for toroid-cone shaped cutters. Int J Adv Manuf Technol 29(9–10):912–921
17. Chen F, Bin H (2009) A novel CNC grinding method for the rake face of a taper ball-end mill with a CBN spherical grinding wheel. Int J Adv Manuf Technol 41(9–10):846–857
18. Karpuschewski B, Jandecka K, Mourek D (2011) Automatic search for wheel position in flute grinding of cutting tools. CIRP Ann—Manuf Technol 60:347–350. doi:10.1016/j.cirp.2011.03.113
19. Rababah MM, Chen ZC (2013) An automated and accurate CNC programming approach to five-axis flute grinding of cylindrical end-mills using the direct method. J Manuf Sci Eng 135:011011. doi:10.1115/1.4023271
20. Wang L, Chen ZC, Li J, Sun J (2015) A novel approach to determination of wheel position and orientation for five-axis CNC flute grinding of end mills. Int J Adv Manuf Technol 84:2499–2514. doi:10.1007/s00170-015-7851-2
21. Ren L, Wang S, Yi L, Sun S (2016) An accurate method for five-axis flute grinding in cylindrical end-mills using standard 1V1/1A1 grinding wheels. Precis Eng 43:387–394